AD_____

Award Number: W81XWH-04-1-0229

TITLE: Non-Invasive Monitoring for Optimization of Therapeutic Drug Delivery by Biodegradable Fiber to Prostate Tumor

PRINCIPAL INVESTIGATOR: Dan Popa, Ph.D.
Hanli Liu, Ph.D.
Liping Tang, Ph.D.

CONTRACTING ORGANIZATION: The University of Texas at Arlington
Arlington, TX 76019

REPORT DATE: February 2006

TYPE OF REPORT: Annual

PREPARED FOR: U.S. Army Medical Research and Materiel Command
Fort Detrick, Maryland 21702-5012

DISTRIBUTION STATEMENT:

□ Approved for public release; distribution unlimited

# REPORT DOCUMENTATION PAGE

*Form Approved*
*OMB No. 0704-0188*



| 1. REPORT DATE | 2. REPORT TYPE | 3. DATES COVERED |
|---|---|---|
| 01-02-2006 | Annual | 21 Jan 2005 – 20 Jan 2006 |

**4. TITLE AND SUBTITLE**

Non-Invasive Monitoring for Optimization of Therapeutic Drug Delivery by Biodegradable Fiber to Prostate Tumor

**5a. CONTRACT NUMBER**

**5b. GRANT NUMBER**
W81XWH-04-1-0229

**5c. PROGRAM ELEMENT NUMBER**

**6. AUTHOR(S)**
Dan Popa, Ph.D.
Hanli Liu, Ph.D.
Liping Tang, Ph.D.

**5d. PROJECT NUMBER**

**5e. TASK NUMBER**

**5f. WORK UNIT NUMBER**

**7. PERFORMING ORGANIZATION NAME(S) AND ADDRESS(ES)**

The University of Texas at Arlington
Arlington, TX 76019

**8. PERFORMING ORGANIZATION REPORT NUMBER**

**9. SPONSORING / MONITORING AGENCY NAME(S) AND ADDRESS(ES)**
U.S. Army Medical Research and Materiel Command
Fort Detrick, Maryland 21702-5012

**10. SPONSOR/MONITOR'S ACRONYM(S)**

**11. SPONSOR/MONITOR'S REPORT NUMBER(S)**

**12. DISTRIBUTION / AVAILABILITY STATEMENT**
Approved for Public Release; Distribution Unlimited

**13. SUPPLEMENTARY NOTES**
Original contains colored plates: ALL DTIC reproductions will be in black and white.

**14. ABSTRACT**

Chemotherapeutic Drugs delivered by systematic administration exhibit great toxicity; patients have to endure suffering from frequent injection or low dose IV treatment. Thus controlled release of these drugs will be a treatment modality. Moreover, real-time monitoring of the effects of the drug by sensing the dynamic response of the tumor to a particular drug can significantly enhance the therapeutic outcome. The Hypotheses are (1): A near-infrared (NIR) imager can non-invasively monitor the dynamic and chronic distribution of the chemotherapeutic drug, vascular oxygenation, and blood volumes in prostate tumors. (2): The dynamic response of prostate tumor oxygenation to the chronic drug delivery can serve as indicator for treatment prognosis. The Specific Aims are: (1): To design and implement a NIR spectroscopic imaging system (2): To develop 2D tomographic imaging of drug concentration and tumor oxygenation. (3): to control the delivery of drug and (4): to study the relationship between drug release rate, tumor oxygen levels and therapeutic outcome.

**15. SUBJECT TERMS**
Technology Development, Radiological Sciences, Tumor Therapy Planning and Prognosis, Tumor Physiology Monitoring.

| 16. SECURITY CLASSIFICATION OF: | | | | 18. NUMBER OF PAGES | 19a. NAME OF RESPONSIBLE PERSON |
|---|---|---|---|---|---|
| a. REPORT | b. ABSTRACT | c. THIS PAGE | | | USAMRMC |
| U | U | U | UU | 15 | 19b. TELEPHONE NUMBER *(include area code)* |

## Table of Contents

## 2005-2006 Annual Progress Report (Year II)

This report presents progress and accomplishment during the second year, between March 1 2005 and February 28 2006. A new PI, Dr. Dan Popa from the Electrical Engineering Department was approved in February 2006.

### Introduction

Chemotherapeutic drugs delivered by systematic administration exhibit great toxicity; patients have to endure suffering from frequent injection or low dose IV treatment. Thus controlled release of these drugs will be a treatment modality. Moreover, real-time monitoring of the effects of the drug by sensing the dynamic response of the tumor to a particular drug can significantly enhance the therapeutic outcome. The Hypotheses are (1): A near-infrared (NIR) imager can non-invasively monitor the dynamic and chronic distribution of the chemotherapeutic drug, vascular oxygenation, and blood volumes in prostate tumors. (2): The dynamic response of prostate tumor oxygenation to the chronic drug delivery can serve as indicator for treatment prognosis. The Specific Aims are:
**(Aim 1)**: To design and implement a NIR spectroscopic imaging system
**(Aim 2)**: To develop 2D tomographic imaging of drug concentration and tumor oxygenation.
**(Aim 3)**: To control the delivery of drug using both biodegradable fibers, and a novel implantable micropump (IDDS).
**(Aim 4)**: To study the relationship between drug release rate, tumor oxygen levels and therapeutic outcome.
**(Aim 5)**: To create appropriate cancer tumor animal models, that will guide the growth of cancer tumor in Copenhagen rats.

### Body of Report

**Aim 1:** to design and implement an 8-source, 8-detector, NIR spectroscopic imaging system suitable for dynamic imaging of drug concentrations, tumor oxygenation, and tumor blood volume.

Originally, our aim was to design and implement an 8-source, 8-detector, NIR spectroscopic imaging system. To improve the spatial resolution of the dynamic images, in principle, more sources and detectors are needed. For this purpose, we designed and implemented a CCD-camera based, NIR spectroscopic imaging system, partially because of extra funding that co-investigator (co-I) Liu has obtained. With this new approach, the spatial resolution for dynamic images of tumors under treatment can be improved significantly.

### CCD Camera Implementation and Calibration

Implementation and Characteristics of the CCD Camera
Since 2004, co-I Liu has closely worked with Apogee Biodimensions, a medical imaging company, to design and implement a multi-spectral, high-speed CCD camera in order to image dynamic light scattering during neural activities. Figure 1 shows a photo of our current CCD camera attached with a mechanical wheel holding six spectral filters at the NIR range. This system allows us to acquire 6-spectral images to quantify both light scattering and absorption of the measured sample.

The spatial resolution of the camera depends on the selection of the field of view; the typical pixel size in our study is about 20x20 $\mu m^2$. To statistically smoothen out the random noise due to Brownian motion of various scatterers in tissue, we can bin multiple pixels for a local point reading to achieve a sub-mm spatial resolution. The temporal resolution of our current camera, on the other hand, is ~ 50 ms per image frame if a fixed filter is chosen and utilized. By choosing a smaller region of interest, the image acquisition rate can be improved further to obtain 20 ms per frame. When the six filters are utilized, the complete cycle of 6 spectral images takes ~15 seconds. We normally take multi-spectral images during the baseline recording time to obtain static values of both light scattering and absorption parameters.


**Figure 1.** A fast 12-bit CCD camera with a mechanical wheel attached at the camera head.

Laboratory Calibration for Determination of Light Scattering and Absorption from the CCD Camera

In order to separate the effects between light scattering from absorption for the CCD imaging data, we developed an empirical approach. We can start with eq. (1) for the light reflectance taken from the CCD camera:

$$R(\mu_a, \mu_s') = \frac{\Psi(I_0, \mu_s') \cdot (\mu_s')^2}{4\pi} \exp(-z_0 \mu_{eff}) \quad (1)$$

where $\mu_a$ and $\mu_s'$ are light absorption and scattering coefficients, $\mu_{eff}=(3\mu_a\mu_s')^{0.5}$, $z_0=1/\mu_s'$, and $\Psi(I_0, \mu_s')=\Psi_{CCD}(I_0, \mu_a, \mu_s')$ is the calibration term for the CCD camera and needs to be obtained from the laboratory phantom measurements. In our previous study for a needle probe, we proved that $\Psi(I_0, \mu_a, \mu_s')$ is a function of only $\mu_s'$, not strongly depending on absorption. For CCD camera calibration, we performed the experiments as described below:

3 liters of intralipid solution in a large container were imaged using the multi-wavelength CCD camera. The images were obtained for the following intralipid concentrations: 0.5 %, 0.8 %, 1.0%, 1.2%, 1.5%, and 2.0% and also 1.0% intralipid with 1.0, 1.5, and 2.0 ml of ink or (horse blood) mixed with it, as shown in Figures 2(a) and 2(b). Optical parameters of the solution, $\mu_a$ and $\mu_s'$, from a standard spectrometer (the ISS oximeter) were obtained before imaging. The camera was mounted on top of the solution and a light from a broadband light source was focused on the intralipid solution in such a way that there is uniform illumination. Care was taken to mark the height between the camera entrance and the surface of the liquid. This was to ensure that there was no difference in successive experiments and it was easily repeatable. The camera was then adjusted (e.g., focus distance and slit width) to obtain a clear image of the intralipid solution. 10 images from a particular filter were taken, and all images were obtained at the same integration time (90ms).

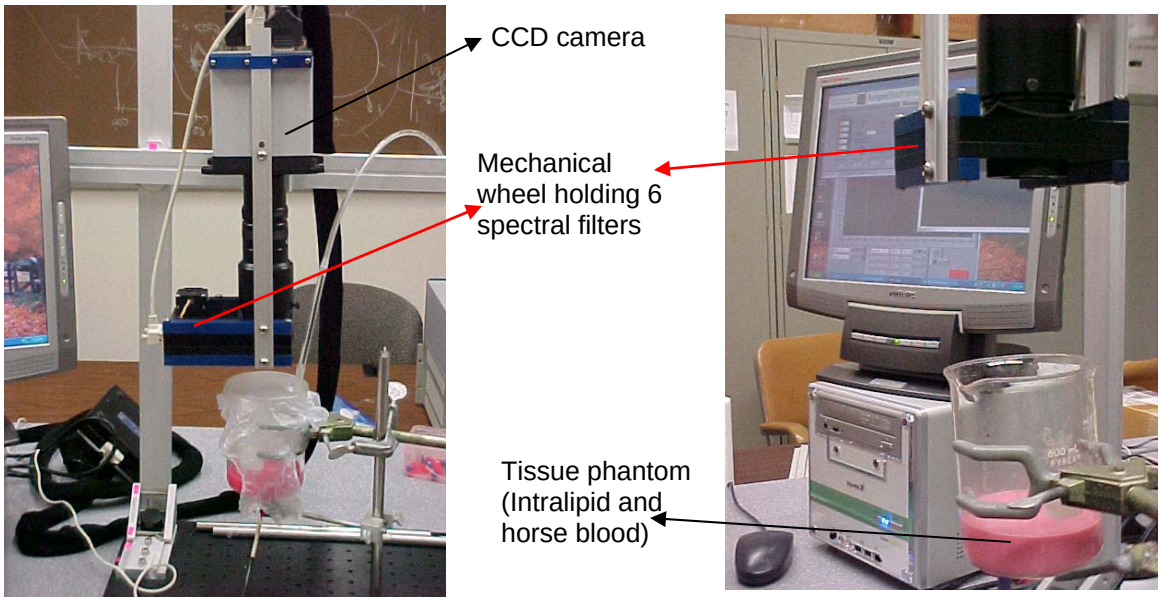


**Figure 2(a)** Experimental setup of the CCD camera for the laboratory phantom study.

**Figure 2(b)** A close look of the CCD camera head with the Intralipid solution mixed with horse blood.

After the CCD readings were recorded, we averaged them across the entire images, as functions of $\mu_a$ and $\mu_s$' by measuring ink and Intralipid concentrations, respectively. Figures 3(a) and 3(b) show that $\Psi_{CCD}(I_0, \mu_a, \mu_s')$ has an power dependence on $\mu_s$' and a linear relationship on $\mu_a$.

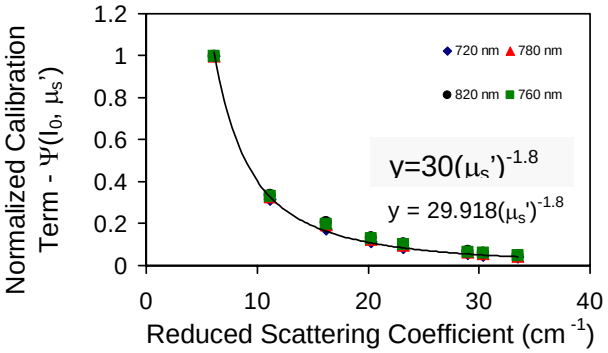


**Figure 3(a)** The empirical relationship between $\Psi_{CCD}(I_0,\mu_a,\mu_s')$ and $\mu_s$', having a power of $(\mu_s')^{-1.8}$.

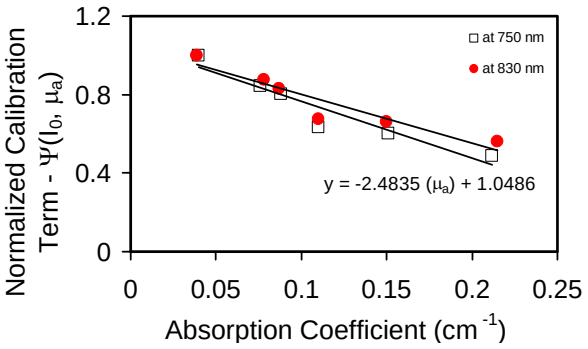


**Figure 3(b)** The empirical relationship between $\Psi_{CCD}(I_0,\mu_a,\mu_s')$ and $\mu_a$, having a linear relationship.

Based on the preliminary results given above, we then express $\Psi_{CCD}(I_0, \mu_a, \mu_s')$ as

$$\Psi_{CCD}(I_0, \mu_a, \mu_s')=f(\mu_s')\, g(\mu_a) = \alpha\, (\mu_s')^{-1.8}(\mu_a+\beta), \quad (2)$$

where $\alpha$ and $\beta$ are two empirical parameters that can be calibrated from the laboratory phantoms and be later utilized for quantification of $\mu_a$ and $\mu_s$' of the rat prostate tumors so as to quantify hemodynamic responses to the therapy.

**Aim 2:** to develop a 2D tomographic reconstruction algorithm, so as to obtain 2D tomographic images of tumor vascular oxygenation and the drug concentration delivered through the biodegradable fiber.

Right now, we are in the process of developing the 2D tomographic reconstruction algorithm for the CCD camera data.

**Aim 3:** To control the delivery of drug. This can be done using both biodegradable fibers, and a novel implantable micropump (IDDS). In this report we describe research towards developing an implantable drug-delivery system (IDDS).

Micropumps play a key role in microfluidic circuits where nano or pico-liter volumes of fluid are delivered and controlled for applications to biotechnology, drug discovery and drug delivery. In general, diaphragm driven pumps have self-priming advantages compared to electrically driven pumps, and a variety of actuation principles, valve mechanisms and fabrication processes have been used to build diaphragms. Current pump designs consist of multiple layers, where each layer has a unique function, such as a diaphragm, valve, or actuator. However, multiple layer structures require expensive wafer alignment and bonding as well as externally assembled actuators.

From several discussions with physicians involved in treating cancerous tumors, it is evident that the addition of an implantable micropump would alleviate a lot of the discomfort suffered by patients using available treatments. Currently, most patients are administered cancer-fighting drugs through an external pump, which means that they must remain immobilized for extended periods of time. The benefits of a small, implantable delivery system will also include the ability to precisely control drug dosage over the many days required for treatment.

We have prototyped a novel, monolithically fabricated micropump referred to as an in-plane micropump. This pump includes three major components: a diaphragm, an actuator, and a valve, all in a single layer as shown in Figure 5. The pump is part of a packaged IDDS unit including a sub-cutaneous port reservoir, microfluidic interconnects, on-board power and control circuitry as shown in the diagram in Figure 4.

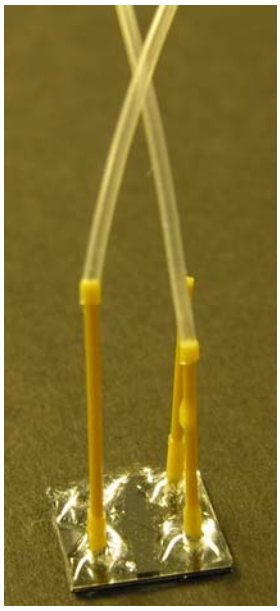

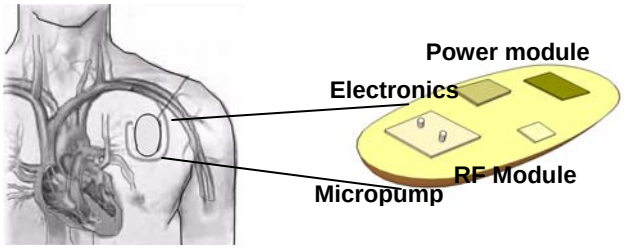


**Figure 4.** Schematic diagram of Implantable drug delivery system (IDDS) module (top) and packaged and interconnected micropump (left)

The pump consists of electrothermal actuators, a lever mechanism to amplify the stroke, a diaphragm, and inlet and outlet check valves. The DRIE (Deep Reactive Ion Etching) process was used to fabricate the pump structure on a highly

doped SOI (Silicon-On-Insulator) wafer, and wafer bonding was used to cover the pump structure with a glass wafer. The electrothermal actuator consists of a bank of thin silicon rib structure, which thermally expands when electrical power is applied. The rib expansion drives a lever mechanism that pulls or pushes the diaphragm. This mechanism increases the compression ratio for a better self-priming capability. The compression raito of the current prototype is 3.5 to 1. Other operating characteristics are: 5 to 15 volt range for the pump, and a maximum flow rate of 100μl/min at 100Hz input. The new in-plane micrompump reduces pump size and manufacturing complexity. The die level pump size is 2(W)x4(L)x1.5(T)mm$^3$. The embeded actuator eliminates the need to externally assembe an actuator, and the monolithic structure reduces the need for high cost alignment and wafer level bonding. In this document we argue that this micropump can be manufactured at relatively low cost for applications such as implantable drug delivery systems.

Implantable drug delivery systems (IDDS) are not new [6,8,14,15], however they have not been previously used for the treatment of cancer. Previous research involving implantable micropumps includes three types of actuation principles: piezoelectric [13], silicon MEMS electrostatic or electrothermal [9,11,13] and shape memory alloys (SMA) [12]. Some implantable micropumps have been used to deliver pain relief medication or insulin, and some are commercially available [14-15]. At present, the cost of an implantable insulin delivery system is still prohibitively high, while its long-time reliability is questionable [8]. Furthermore, the treatment benefits of an implantable insulin delivery system have not yet been demonstrated in clinical trials and might not exceed those of external pumps, stents, or slow release micro and nano-capsules [7-8].

However, the benefits of an IDDS are apparent in the case of cancer treatment, in particular prostate cancer. Such treatments often require continuous delivery of cancer drugs once a week. The delivery can take place over 24-48 hour period, after which there is no treatment for the rest of the week. Current delivery methods include intravenous pumping and drug injection. If the cancer is at the surface of an organ, drugs delivered directly to that surface might work well, otherwise, and this is the case with most cancers, it is best to deliver the drug using the blood stream. In order to reduce the quantity of drug administered, it is possible to target arteries close to the affected organ, but there is always a risk for metastasis. Furthermore, if the cancer is hard to reach, the drug can be injected directly into the tumor, but this is less reliable and less effective than blood delivery. An exploded drawing of the pump assembly is shown in Figure 5.

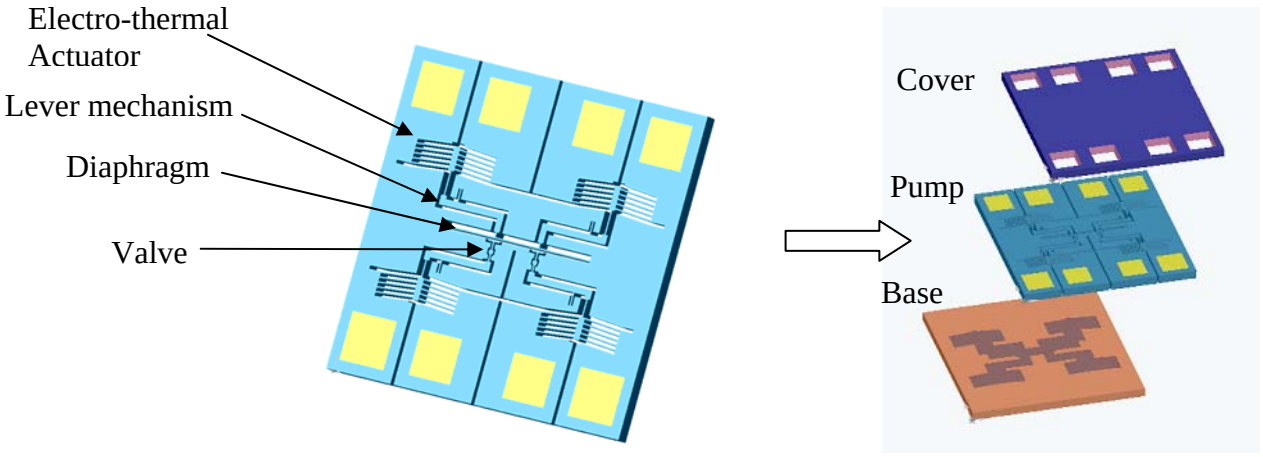


**Figure 5.** In-plane micropump. (a) An exploded view of a 3-layer design. (b) A micropump that has actuator, diaphragm and valves on a single die

The middle silicon layer has thermal actuators, a lever mechanism, a pump diaphragm, and check valves. The cover and base silicon plates are assembled with the pump layer to enclose the fluidic parts. The actuation mechanism of the pump is electro-thermo-mechanical. The actuator consists of ribs of thin silicon, which expand by means of Joule electrical resistance heating. When electrical voltage is applied to the actuator, the ribs expansion pulls a rigid bar that is pivoted by a thin flexible bar. The rigid bar works as a lever mechanism to amplify the motion of the thermal actuator. Single or multiple actuators can be used to add greater force, and this figure shows two thermal actuators are used to actuate the pump diaphragm. The diaphragm bends with the motion of the rigid bars in the pump chamber. The amount of diaphragm deflection affects the volume of intake and compression, therefore flexible diaphragm is necessary to create high compression ratio.

The middle pump layer is stacked together with a top cover plate and a bottom base plate. A few micron step structure is engraved on both the cover and base plate to allow small gaps between the plates and moving parts of the pump layer. The cover plate has through-holes, which are used for electrical interconnections of the pump layer. The base plate has through-holes for fluidic interconnection between the pump chamber and outside of the pump.

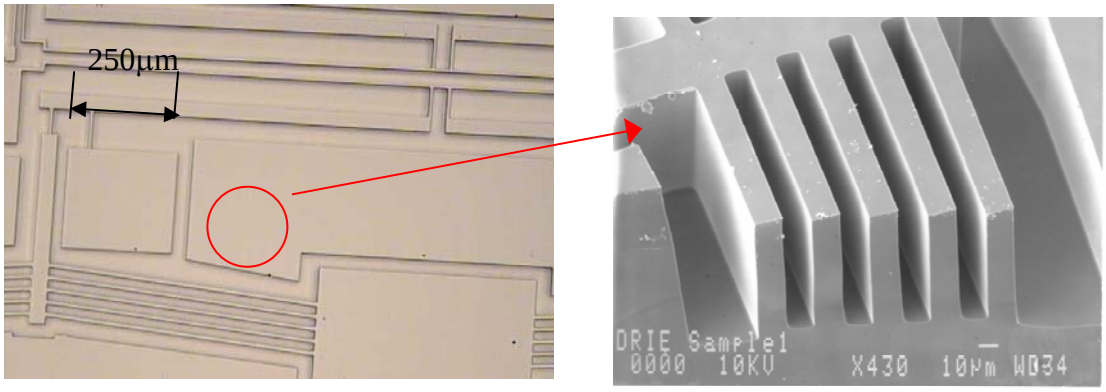


**Figure 6.** DRIE micromachined micropump structure. (a) In plane micropump. (b) SEM image of cross section of an electrothermal actuator.

The mechanical performance of the pump is simulated using both Finite Element Analysis (FEA) as well as a lumped model approximation. The results are shown in Figure 7. The simulation shows that the temperature at the center of the actuator is most hot region and it goes down quickly toward to the diaphragm.

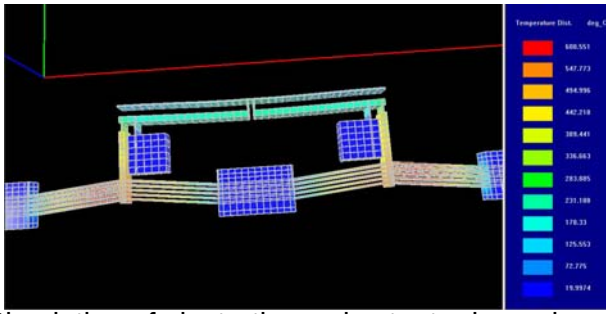

**Figure 7.** Simulation of electrothermal actuator in a micropump.

The simulation model was used to finalize the pump geometry prior to fabrication. Actual experiments were then performed to characterize the electrothermal actuators. The actuation mechanism consumes about 0.5W power, and it provides about 40μm stroke with an incorporated diaphragm. The full pump specifications are shown in Table 1.

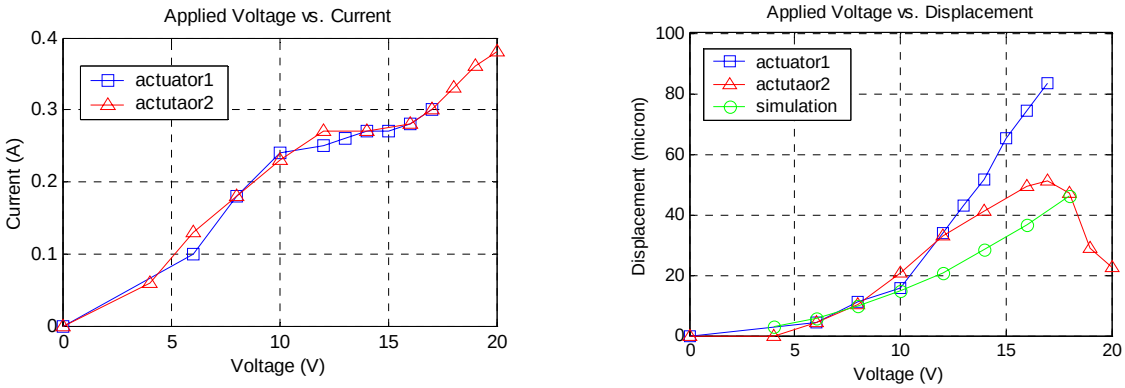


**Figure 8.** Characterization of MEMS actuators. (a) Power consumption (b)

| Parameter | Specification |
|---|---|
| Dimension | 4mm×2mm×1.5 |
| Pumping volume | 3.6nL (chamber volume) |
| Compression ratio | 3.5 |
| Flow rate | ~100μL/min |
| Back pressure | |
| Operating frequency | 1~100Hz |
| Operating voltage | 5~10V |
| Power consumption | 0.5W |

**Table 1.** Specifications of in-plane micropump.

We are currently in the process of packaging and testing the IDDS system.

**Aim 4:** to study the relationship among the drug release rate, tumor oxygenation and therapeutic outcome, so as to obtain optimal conditions for efficient drug delivery and better therapy outcome.

For this aim, we started our animal measurements using the CCD camera. Figure 9(a) shows the setup of the CCD camera, and the relative position between the camera and rat tumor. Figure 9(b) shows a close look of the rat prostate tumor and four fiber bundle tips that were used to deliver light. The prostate tumor line was R3327 AT3.1, and it generally took 7-10 days to have the tumor appear on the animal foreback.

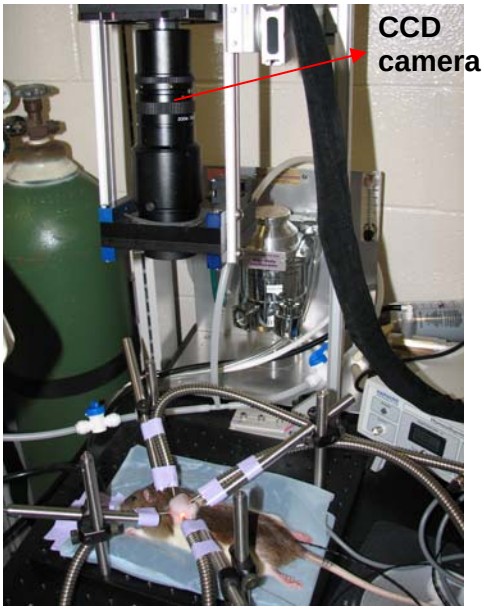


**Figure 9(a)** Experimental setup for animal study.

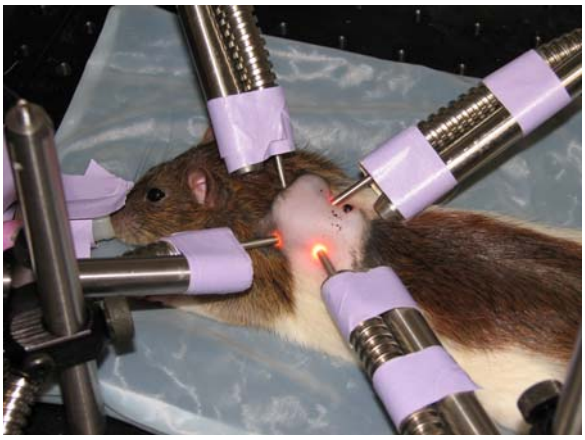

**Figure 9(b)** A Coperhagen rat with a prostate tumor grown on the foreback. Four light-delivery fiber bundles are in good contact with the tumor for the NIR measurement. The four probes were held through the metal optical posts, as shown.

A dosage of 200 mg of Cyclophosphamide (Sigma-Aldrich, Inc) per kilogram of rat body weight was initially used to investigate the primary effects of the drug. The drug was injected through ip when the tumors appeared to be 1.5 cm in diameter. Continuous recordings on the animals' tumor size and body weight were done daily after the drug injection. Figures 10 (a) and (b) show the corresponding changes in tumor volume and percentage decrease in rat body weight, for two control rats and two treated rats. It appears that the treated rats have a slower rate in tumor grow and in body weight lose in comparison to the control rats. It also suggests that the dosage of drug seems to be a little low, and it is reasonable to expect that a higher dosage of drug could stop the tumor grow. However, whether or not a higher dosage would lead to a toxic effect on the animal remains to be investigated through the rest of the funding period. We are currently carrying out the continuous study with more animals and more detailed measurements.

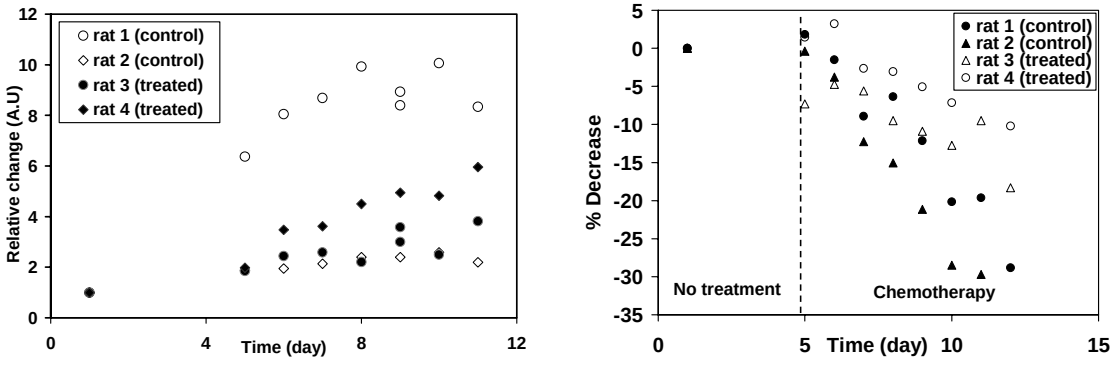


**Figure 10.** Changes in tumor volume with time (a) and changes in rat body wt. with time (b)

Furthermore, we employed the CCD camera, as shown in Figures 3(a) and 3(b), to detect and quantify the hemodynamic changes of the prostate tumors under oxygen

intervention. The protocol for oxygen intervention is given as follows: 10 minutes for baseline recording while the rat breathed air, followed by 10 minutes of oxygen breathing for the rat, and then switched back to air for another 10 minutes. We expect to see different dynamic responses to oxygen intervention between control and treated rat tumors, and such dynamic responses can provide us with information on therapeutic effects and efficacy of the drug. Figure 11 shows an example of such a hemodynamic response of a prostate tumor to oxygen, and this figure is obtained by averaging the tumor region.

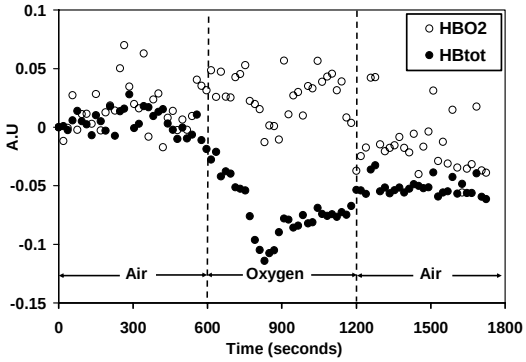


**Figure 11. Hemodynamic changes in the tumor region during gas intervention**

Furthermore, Figures 12(a) and 12(b) illustrate topographic maps of oxygenated hemoglobin concentration of the tumor during the periods of baseline and oxygen intervention, respectively. Figure 8(b) basically shows that some regions of the tumor have a large increase in oxygenated hemoglobin (HbO), represented by red color, and some regions do not show (or have small) changes in HbO. The color scale given on the right hand side of Figure 12(b) gives the quantitative representation of the HbO values, while the values of the color scale are in arbitrary unit for a relative comparison. In short, both Figures 11 and 12 basically demonstrate that we have established an effective imaging tool to be used in studying tumor heterogeneity in response to chemotherapy and the relationship among the drug dosage, tumor oxygenation and therapeutic outcome. We will continue making our effort in this direction for the rest of funding period.

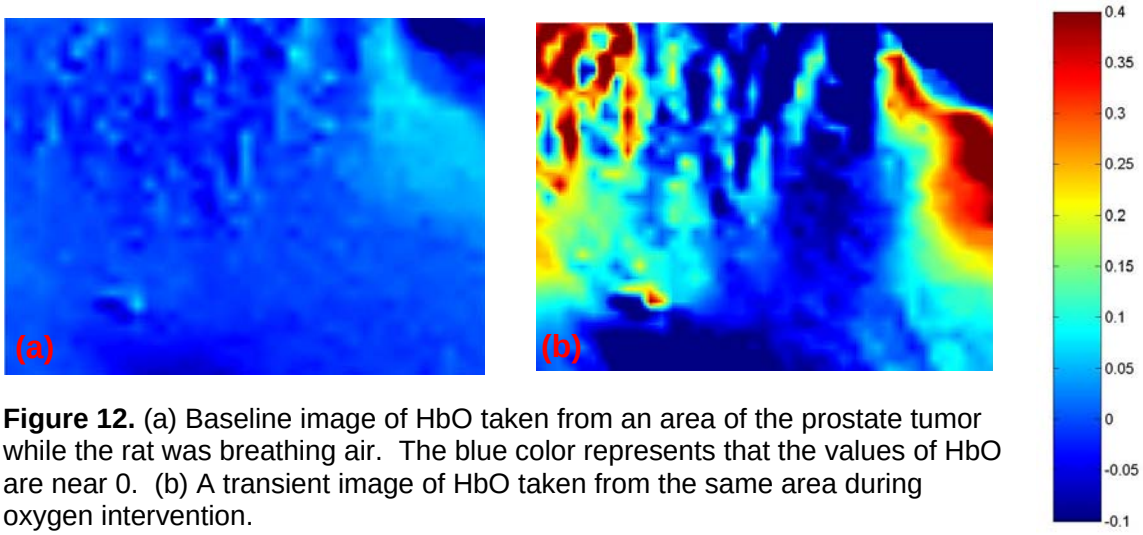


**Figure 12.** (a) Baseline image of HbO taken from an area of the prostate tumor while the rat was breathing air. The blue color represents that the values of HbO are near 0. (b) A transient image of HbO taken from the same area during oxygen intervention.

**Aim 5:** To create appropriate cancer tumor animal models, that will guide the growth of cancer tumor in Copenhagen rats. These rats are then used to support all the experimental work in the project.

For the past 12 months, we have successfully established reproducible prostate cancer animal model using cancer cell lines. Many of these animals have been used in the study of the development of imaging modality. Specifically, rat prostate cancer cell line R-3327-AT-3.1 was obtained from the American Type Culture Collection (Rockville, MA, USA). Cells were cultured in Dulbecco's Modified Eagle Medium DMEM supplemented with 10% Fetal Bovine Serum (Invitrogen, CA, USA) at 37˚C in a 100% humidified atmosphere containing 5% carbon dioxide. The subcultivation ratio is 1:20 and the medium was changed every other day to ensure the fast growth of the cells.

The prostate cancer cells are adherent cells, have spindle-like shape and grow really fast (Figure 13). The cells were subcultured when they reach 80% confluence (~ once every 4 days). Some of the cells were cryo-preserved in liquid nitrogen.

To create prostate tumor in animals, we used male Copenhagen rats with 150 grams body weight. R-3327-AT-3.1 cells were recovered from culture flasks and then adjusted to $1\times10^7$/ml in PBS. Prior to implantation, rats were anesthetized with the inhalation of 1-3% of isoflurane and then shaved to expose back foreside skin. Following sedation, 100µl of cell solution (equivalent to ~ $1\times10^6$ R-3327-AT-3.1 cells) were injected subcutaneously under the foreside skin. In about 7 to 8 days, tumor tissues were growing to ~0.5-1.0cm diameter which is the perfect size for our imaging study. If needed, tumor growth rate would be reduced by injecting lesser R-3327-AT-3.1 cells. Similar tumor can also be created by implantation prostate tumor tissue freshly isolated from other animals. Our results have shown that the implantation of tumor tissue has worse reproducibility than injection of cancer cells.

To ensure the quality of our cancer tissue, we often carried out H&E histological examination of the implanted prostate tumor tissue (Figure 14). Typically, prostate tumors possess the following characteristics: rapid cell growth, dense cell tissue, and good microvascular density. We believe that this animal model provides excellent in vivo system to study the imaging modality proposed in this project.

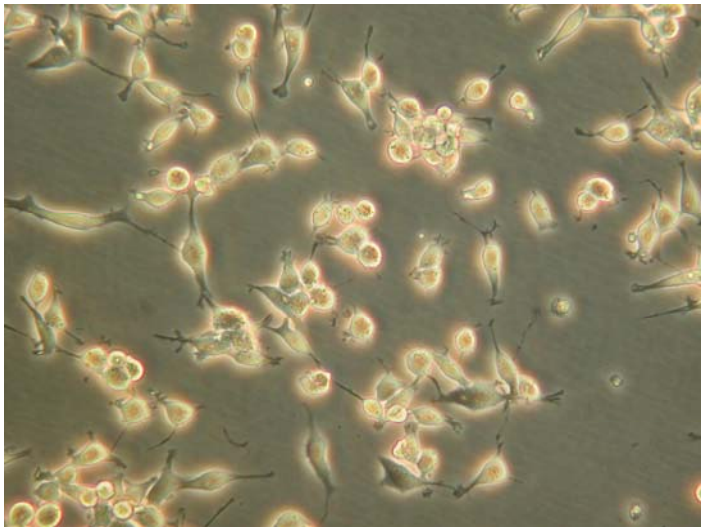

**Figure 13.** Morphology of R-3327-AT-3.1 (low density) under phase contrast microscope, 24 hours after being thawed from liquid nitrogen, 200X..

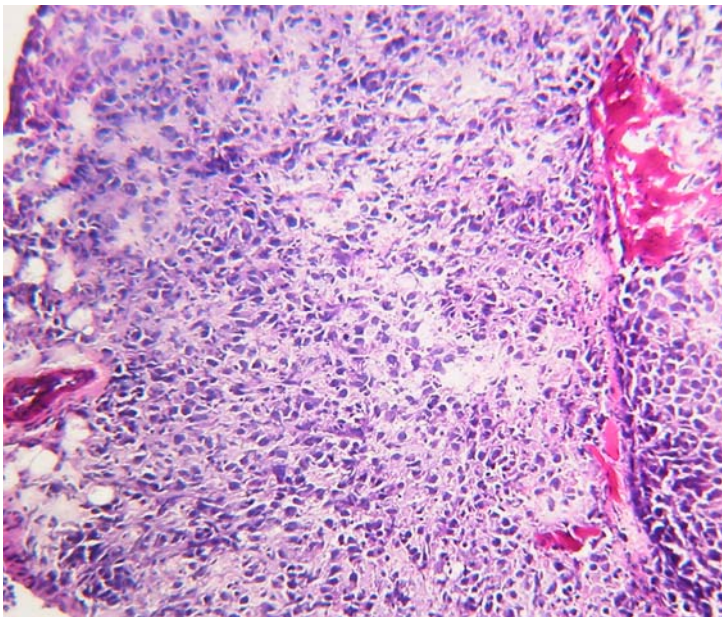

**Figure 14.** Histology of R-3327-AT-3.1 tumor tissue, H&E staining, 100X.

## Key Research Accomplishments

- We have setup and calibrated a blood oxygenation measurement system using a high speed CCD camera to study the evolution of tumors.
- We have designed and fabricated a novel micropump for controlled drug delivery of cancer drugs.
- We have developed animal models for cancer tumor growth.

## Reportable Outcomes

During the second year, this grant supported several graduate students during their M.S. and Ph.D. studies. It supported the completion of a M.S. Thesis and the publication of four conference papers. One of the conference papers (Paper #1) received Best Paper Award at the TexMEMS VII conference held in El Paso, Texas in September 2005.

**M.S. Thesis:**

Amit Mhatre, “IMPLANTABLE DRUG DELIVERY SYSTEM WITH AN IN-PLANE MICROPUMP,” BioMedical Engineering Department, UTA, December 2005.

**Conference Papers:**

1. Smitha M.N.Rao, Amit Mhatre, Dan O Popa, J. C. Chiao, T. Ativanichayaphong, J. Sin and H.E. Stephanou. "MEMS-based Implantable Drug Delivery System, " in Proc. of TEXMEMS VII Conference, El Paso, Texas, September 2005,

2. Ashutosh Kole, Karishma Bushan, Jeongsik Sin, Woo Ho Lee, Dan Popa, Dereje Agonafer and Harry Stephanou. "Polymer Tube Embedded In-Plane Micropump, " in Proc. of TEXMEMS VII Conference, El Paso, Texas, September 2005.

3. Manan Goel, Harsha Radhakrishnan, Liping Tang, and Hanli Liu, "Application of Near Infrared Multi-spectral CCD Imager to Determine the Hemodynamic Changes in Prostate Tumor, " in proc of *Biomedical Optics Topical Meeting*, March 19-March 23, 2006, Fort Lauderdale, Florida.

4. Dheerendra Kashyap, Hanli Liu, "Absolute Quantification of Hemoglobin Derivative Concentrations and Reduced Scattering Coefficients from Turbid Media using Steady State Reflectance Spectroscopy with Single Source-Detector Separation, "in proc of *Biomedical Optics Topical Meeting*, March 19-March 23, 2006, Fort Lauderdale, Florida.

**Students supported:**

Sharman, Vikrant, 3/05 – 5/05
Kashyap, Dheerendra, 07/05 - 08/05
Gorthi, Sankar, 03/05 – 01/06
Goel, Manan, 3/05 – 5/06
Nair, Ashwin, 01/06 – 05/06
Radha, Krishnan, 01/06 – 05/06
Rao, Smitha, 6/05 – 5/06

## References


[1] R. Linnemann, P. Woias, C.-D. Senfft, and J.A. Ditterich, "A self-priming and bubble-tolerant piezoelectric silicon micropump for liquids and gases," Proceedings on The Eleventh Annual International Workshop on Micro Electro Mechanical Systems, pp. 532-537, 1998.

[2] F.K. Forster, R.L. Bardell, M.A. Afromowitz, N.R. Sharma, and A. Blanchard, "Design, fabrication and testing of fixed-valve micro-pumps," Proceedings of the ASME Fluids Engineering Division, pp. 39-44, 1995.

[3] C. Grosjean and Y.-G. Tai, "A thermopneumatic peristaltic micropump," International Conference on Solid-State Sensors and Actuators, 1999.

[4] D. Maillefer, S. Gamper, B. Frehner, and P. Balmer, "A high-performance silicon micropump for disposable drug delivery systems," The 14th IEEE International Conference on MEMS, pp. 413-417, 2001.

[5] J. Sin, W.H. Lee, and H. Stephanou, "In-plane micropump: Design Optimization", in Proc. NSTI Nanotech '04 conference, Boston, Massachusetts, March 2004.

[6] Thomas J. Smith, et. al., "Randomized Clinical Trials of IDDS with CMM for refractory cancer pain", in Journal of Clinical Oncology, Vol 20, No 19 (October 1), 2002: pp 4040-4049.

[7] S. Zafar Razacki, et. al., "Integrated Microsystems for Drug Delivery", in Advanced Drug Delivery Reviews 56 (2004) 185– 198

[8] J. L. Selam, "External and implantable insulin pumps: current place in the treatment of diabetes", in Exp. Clin. Endocrinol Diabetes 109 (2001).

[9] Li Cao, S. Mantell, and D. Polla, "Design and simulation of an implantable medical drug delivery system using MEMS", in Sensors and Actuators 94 (2001).

[10] John T. Santini, et. al., "A controlled-release microchip", in Nature Jan 1999.

[11] A. Grayson, et.al., "Electronic MEMS for triggered delivery", in Advanced Drug Delivery Reviews 56 (2004) 173– 184.

[12] D. Raynerts, "An implantable drug-delivery system based on Shape-Memory-Alloy Micro-Actuation", in Sensors and actuators A61 (1997).

[13] D. Maillefer, et.al., "A high Performance micropump for disposable drug delivery systems", in Proc. IEEE MEMS 2001.

[14] Medtronic Minimed http://www.minimed.com/

[15] Debiotech, S.A., http://www.debiotech.com/